Electronic Supplementary Material (ESI) for Nanoscale.


# Supporting Information for: "Exfoliation of two-dimensional polymer single crystals into thin sheets and investigations of their surface structure by high-resolution atomic force microscopy"

Hannes Beyer,[*a] Max J. Kory,[bc] Gregor Hofer,[b] Andreas Stemmer,[*a] and A. Dieter Schlüter[*b]

[a] *Nanotechnology Group, Department of Mechanical and Process Engineering, ETH Zürich, Säumerstrasse 4, 8803 Rüschlikon, Switzerland. Email: hbeyer@ethz.ch, astemmer@ethz.ch*
[b] *Laboratory of Polymer Chemistry, Department of Materials, ETH Zürich, Vladimir-Prelog-Weg 5, 8093 Zürich, Switzerland. Email: dieter.schlueter@mat.ethz.ch*
[c] *Now at Battrion AG, Sempacherstrasse 15, 6003 Luzern, Switzerland.*

## Contents

# 1 2DP crystal preparation

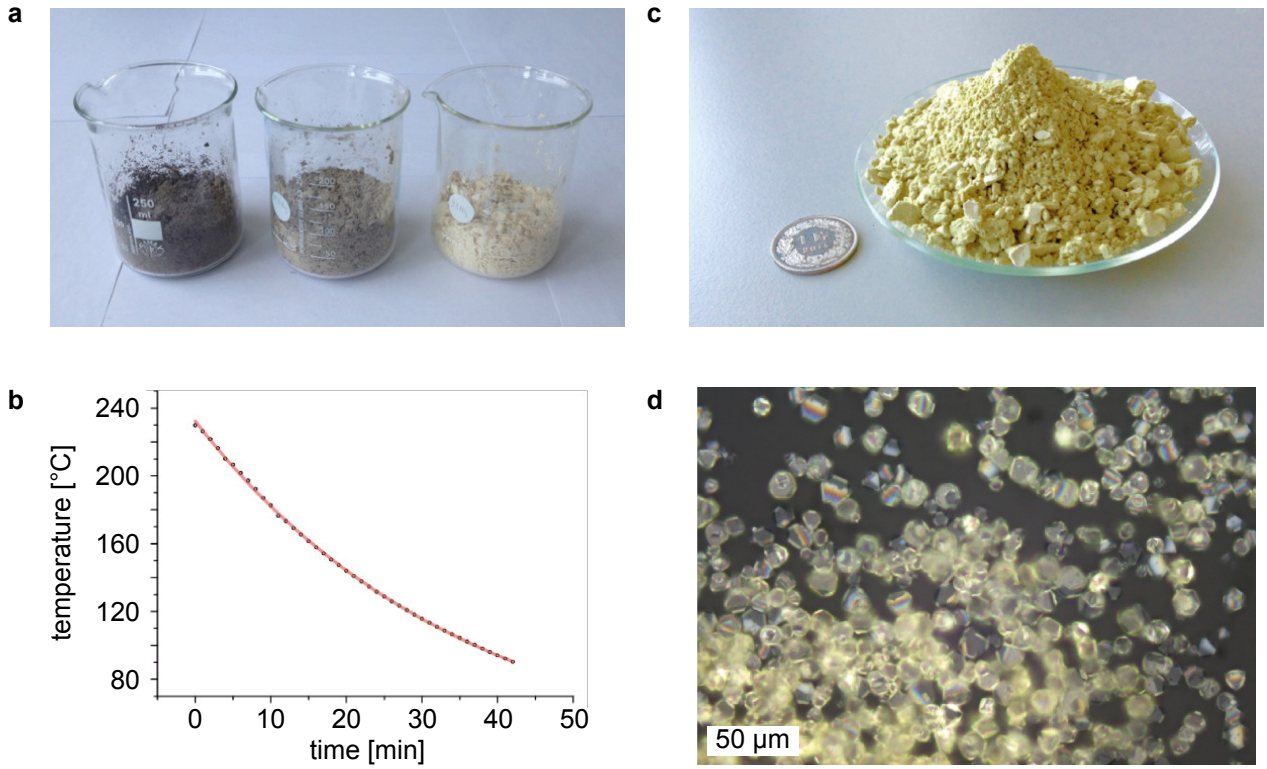


Figure S1: (a) From left to right: after first, second, and third recrystallization from propylene carbonate (PC) (b) Cooling profile to obtain mostly hexagonal shaped crystals as shown in c) and d). (c) Monomer crystals after recrystallization from 2-cyanopyridine. (d) Optical microscopy image of truncated trigonal anti-prismatic crystals (sizes ca. 20 µm).

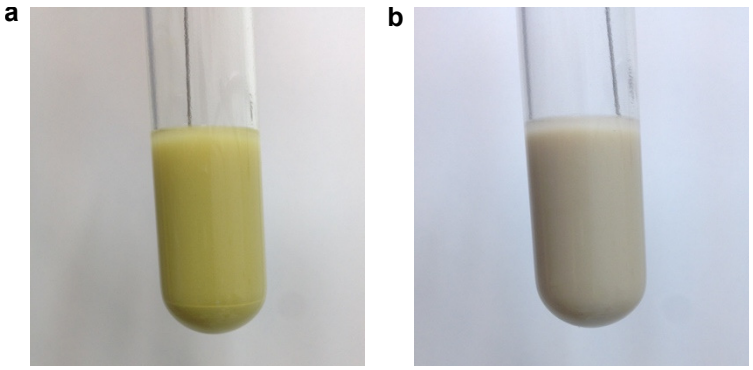


Figure S2: Crystals before (a) and after irradiation (b) with $\lambda$=465 nm.

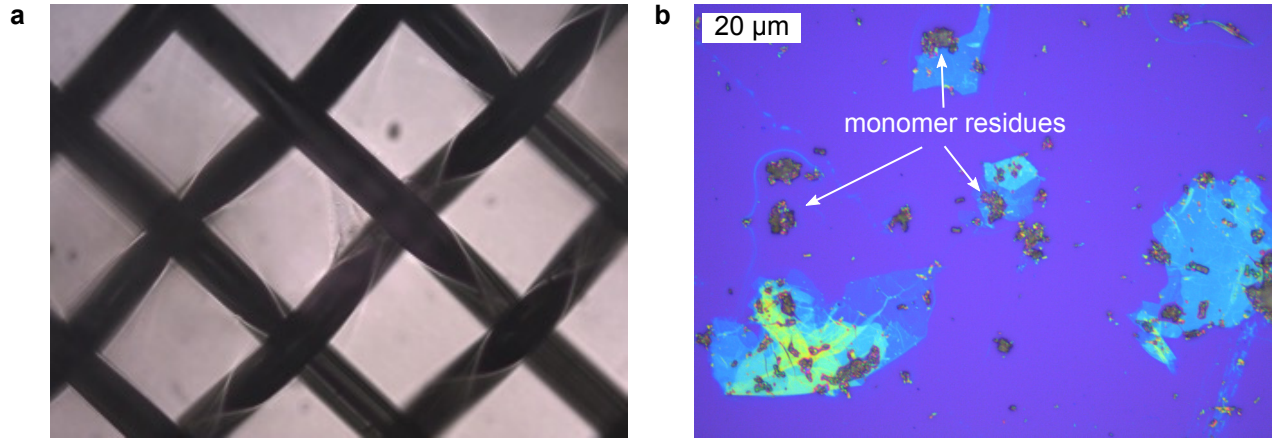


Figure S3: (a) Stainless steel wire mesh with a hole size of 50 µm. (b) Exfoliated type 2 2D polymer sheet stacks and monomer residues on a $SiO_2$(300 nm)/Si wafer. The sample was obtained by directly placing a droplet onto the wafer without filtering it through a stainless steel wire mesh.

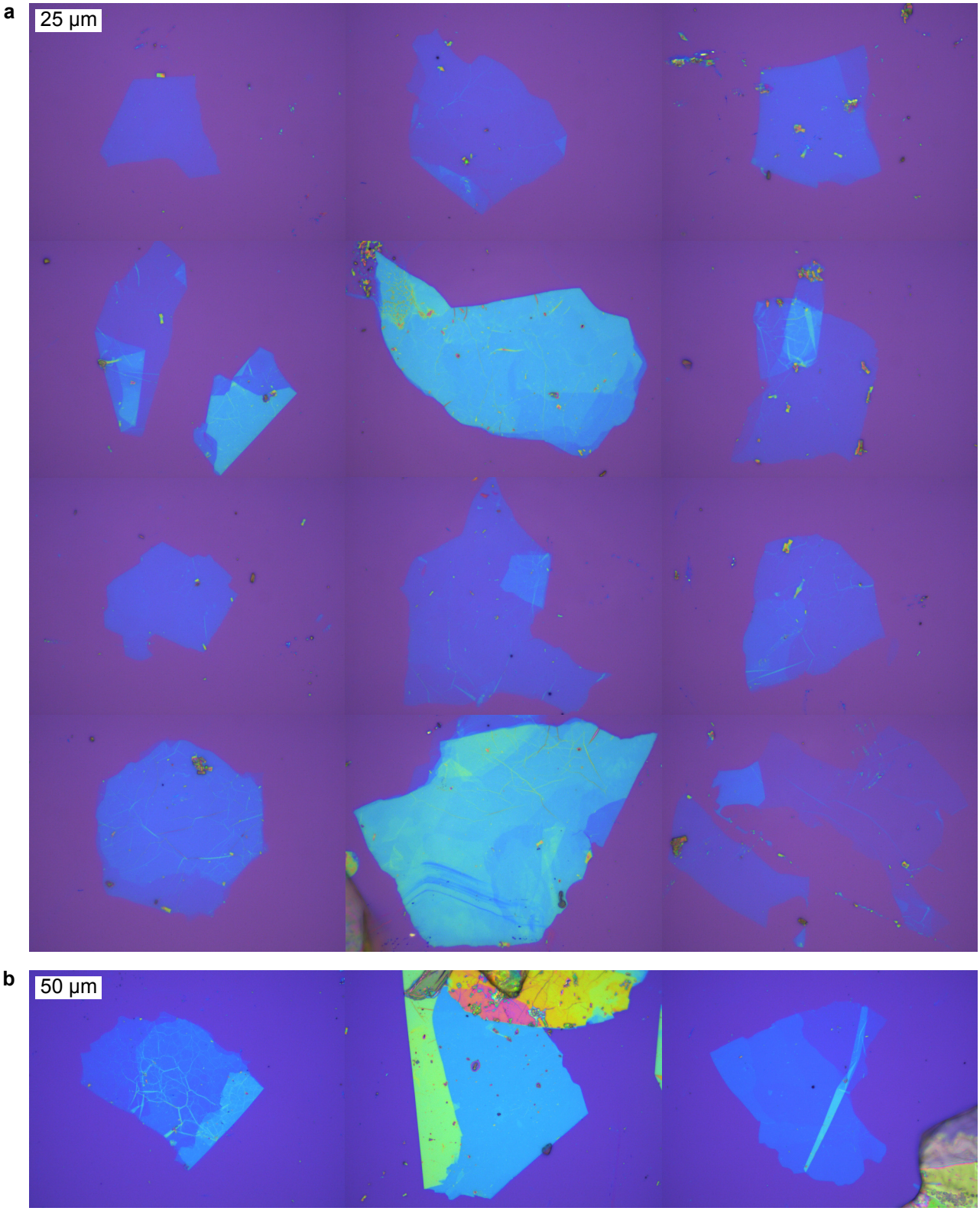


Figure S4: Optical image gallery of liquid exfoliated type 2 2DP crystals at 100x (a) and 50x magnification (b).

## 2 Color code evaluation

In order to quickly identify the thickness of 2D polymer sheet stacks after exfoliation we followed a method often used characterising 2D materials, e.g. graphene or $MoS_2$. This method is based on visible light interference of sheet stacks on the substrate and correlates the thickness of the sheet with its respective color contrast appearing in reflectance optical microscopy images. To this end, exfoliated sheets were transferred onto $SiO_2$(300 nm)/Si wafers and optical images were taken with a camera (Leica DFC-295) mounted on an optical microscope (Leica DM8000M) which is operated in bright field reflectance mode. Before imaging, the white balance of the camera was set by placing a grey card as specimen and taking a picture with the same magnification as used for imaging the 2D polymer sheets. Along with a constant illumination level, this enabled correct color measurements.
The sheets were then imaged by atomic force microscopy (Cypher, Asylum Research) and the thickness determined from AFM images using Gwyddion. First, the image is levelled and the height values are shifted such that the substrate is at zero height. Second, an area of a plateau with similar height is selected and the height distribution extracted. Since the partially exfoliated crystals usually do not exhibit a completely flat surface, largely caused by adsorbates rather than foldings and step edges, the height distribution was fitted with a Gaussian function to obtain an average thickness (see Fig. S5a) for the individual sheet stacks. To correlate the corresponding color to the thickness determined by AFM the same region was selected in the optical image using image analysis software (Gimp) and mean red-green-blue components (*RGB*-values) were extracted from a histogram (see Fig. S5b).

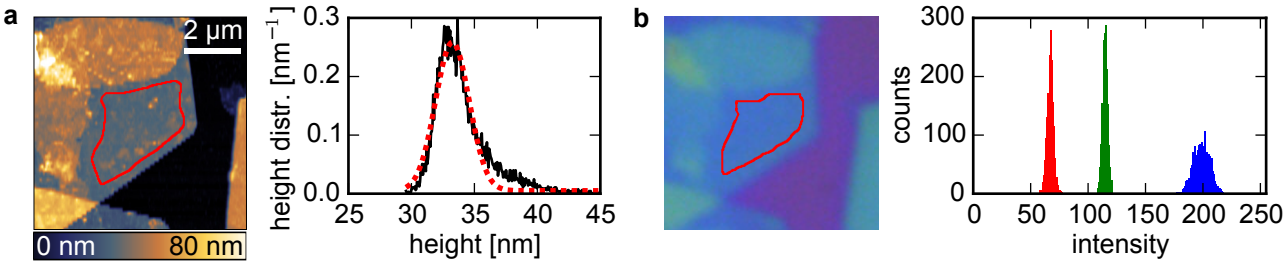


Figure S5: Color code evaluation. (a) AFM topography and height distribution of the area inside the red boundary. The mean height of the Gaussian curve (red dashed) is 33.3 nm. (b) Optical image (no contrast enhancement) of the same area shown in a) and histogram of the individual *R, G, B* channels inside the red boundary. Mean values for *R*, *G*, and *B* are 66.6, 114.4, and 198.3, respectively.

### 2.1 Fresnel's law

The color contrast was also modelled for our optical setup (which can be easily modified to other setups) following Blake et al.[1] who derived the contrast for graphene. From Fresnel's law the reflectance of a thin sheet ($d_1$, $\overline{n}_1$) on a silicon dioxide layer ($d_2$, $\overline{n}_2$) on silicon substrate ($d_3$, $\overline{n}_3$) in air ($d_0$, $n_0$) where $d_i$ and $\overline{n}_i(\lambda)$=$n_i(\lambda)$-i$k_i(\lambda)$ are thickness and complex refractive index of the materials (Fig. S6), respectively, can be calculated to[2]

$$R(\lambda,\varphi) = \left| \frac{r_1 e^{\mathrm{i}(\phi_1+\phi_2)} + r_2 e^{-\mathrm{i}(\phi_1-\phi_2)} + r_3 e^{-\mathrm{i}(\phi_1+\phi_2)} + r_1 r_2 r_3 e^{\mathrm{i}(\phi_1+\phi_2)}}{e^{\phi_1+\phi_2} + r_1 r_2 e^{-\mathrm{i}(\phi_1-\phi_2)} + r_1 r_3 e^{-\mathrm{i}(\phi_1+\phi_2)} + r_2 r_3 e^{\mathrm{i}(\phi_1-\phi_2)}} \right|^2 , \quad (1)$$

with the the phase shifts $\varphi_i$ and Fresnel coefficients $r_i$ for transverse-electric (TE) and transverse-magnetic (TM) polarization:

$$\phi_i = 2\pi\bar{n}_i d_i \cos\varphi_i/\lambda \qquad r_{i,TE} = \frac{\bar{n}_{i-1}\varphi_{i-1} - \bar{n}_i\varphi_i}{\bar{n}_{i-1}\varphi_{i-1} + \bar{n}_i\varphi_i} \qquad r_{i,TM} = \frac{\bar{n}_i\varphi_{i-1} - \bar{n}_{i-1}\varphi_i}{\bar{n}_i\varphi_{i-1} + \bar{n}_{i-1}\varphi_i} \tag{2}$$

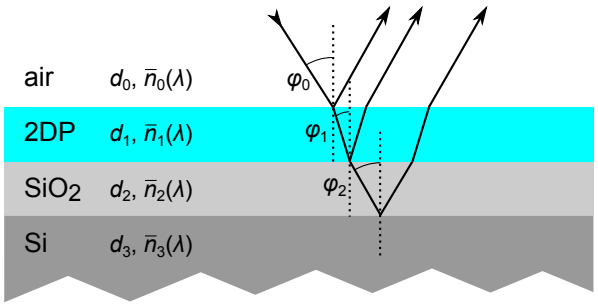


Figure S6: Schematic of the sample surface illustrating reflectance and refraction of incident light at the interfaces.

The complex refractive indices $\bar{n}_2$=$n_2$ ($SiO_2$, only real part) and $\bar{n}_3$ (Si) are taken from literature[3,4], $n_0$=1 for air. The $SiO_2$/Si-wafers used in this study have a thickness of $SiO_2$ $d_2$=300 nm and for Si $d_3$=600 µm. The complex refractive index of the 2D polymer is estimated as follows:
For the extinction $k_1$ of the 2D polymer, optical transmission spectra were measured for several thin crystals deposited on cover glass. The thickness of the crystals was determined by AFM and the extinction coefficient calculated:

$$k = \frac{\lambda}{4\pi}\alpha, \tag{3}$$

whereas $\alpha$, the attenuation coefficient, can be calculated from transmission $T$ and thickness $d$ according to Beer-Lambert law:

$$T = \frac{I}{I_0} = \mathrm{e}^{-\alpha d}. \tag{4}$$

A typical spectrum of the extinction coefficient is presented in Fig. S7 which shows negligible extinction within the visible spectrum. A higher absorption is present at lower wavelength (400 nm). This extinction spectrum (Fig. S7) is used as $k_1$ for the reflectance calculations.

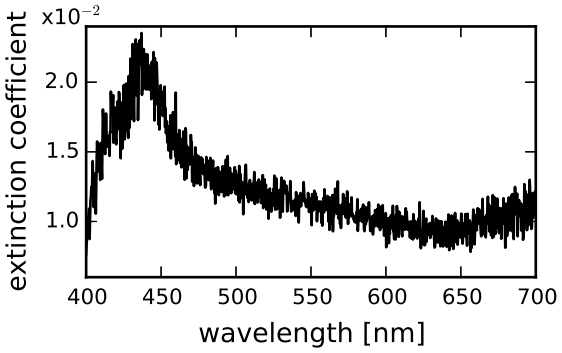


Figure S7: Extinction coefficient derived from transmission spectra of a 61 nm thick 2D polymer.

The real part $n_1$ of the 2DP refractive index was estimated to 1.67-1.7 by refractive index matching using different immersion oils under white light illumination (Becke line method).
Equation (1) gives the reflectance for illumination at a certain angle of incidence $\varphi_i$. In the case of a high magnification objective, e.g. 100X, the numerical aperture (*NA*) is large as well and the assumption of constant angle illumination does not hold. Bruna & Borini[5] have shown that it affects the reflectance considerably. At an *NA* of 0.9, the angle of illumination ranges from 0° (normal incidence) to 64.2° ($\varphi$=arcsin(*NA*)). Numerical integration over the range of illumination angles was therefore performed to include the deviation from normal incidence:

$$R(\lambda) = 2\pi \int_0^{\varphi_m} \mathrm{d}\varphi R(\varphi) W(\varphi) \sin\varphi. \tag{5}$$

As weight function $W(\varphi)$ a Gaussian distribution ($\sigma$=arcsin 0.8 and $\mu$=0, values match the expermiental data best for our setup) was chosen which Bruna & Borini successfully employed to reproduce contrast changes on graphene[5].

## 2.2 Color space transformation

For comparison with the experimentally observed *RGB* color, the modelled reflected spectrum has to be transformed into *RGB* color space as follows:
**(i)** The *XYZ* tristimulus values are calculated by integration of the light reaching the sensor of the camera times the CIE 2006 color matching functions[6] $\tilde{X}_{cmf}$, $\tilde{Y}_{cmf}$, $\tilde{Z}_{cmf}$:

$$\begin{aligned} X &= \int \mathrm{d}\lambda P_{ls}(\lambda) R(\lambda) T^2_{obj}(\lambda) T_{IR}(\lambda) \widetilde{X}_{cmf}(\lambda) \\ Y &= \int \mathrm{d}\lambda P_{ls}(\lambda) R(\lambda) T^2_{obj}(\lambda) T_{IR}(\lambda) \widetilde{Y}_{cmf}(\lambda) \\ Z &= \int \mathrm{d}\lambda P_{ls}(\lambda) R(\lambda) T^2_{obj}(\lambda) T_{IR}(\lambda) \widetilde{Z}_{cmf}(\lambda) \end{aligned} \tag{6}$$

where the light leaving the microscope light source $P_{ls}$ (LED with color temperature 4000 K) passes the objective with a certain transmission spectrum $T_{obj}$, gets reflected $R(\lambda)$, passes the objective again, and finally passes an IR filter $T_{IR}$ before reaching the camera sensor.
**(ii)** Transformation of the source color ($P_{ls}(\lambda)T^2{}_{obj}(\lambda)T_{IR}(\lambda)$) to the destination color (computer screen, standard D65 illuminant) is done by chromatic adaptation. To this end, *XYZ* tristimulus values of the microscope light source with a given white point are transformed to *X'Y'Z'* of the destination light source via a scaling matrix $M_{ca}$ such that the appearance of the colors matches well independent of the light source.

$$\begin{pmatrix} X' \\ Y' \\ Z' \end{pmatrix} = M_{ca} \begin{pmatrix} X \\ Y \\ Z \end{pmatrix}. \tag{7}$$

In this particular step, source white point $X_sY_sZ_s$ and destination white point $X_dY_dZ_d$ tristimulus values are transformed to the cone response domain $\varrho_s\gamma_s\beta_s$ and $\varrho_d\gamma_d\beta_d$ via the Bradford matrix $M_{Brad}$:[7,8]

$$\begin{pmatrix} \varrho_s \\ \gamma_s \\ \beta_s \end{pmatrix} = M_{Brad} \begin{pmatrix} X_s \\ Y_s \\ Z_s \end{pmatrix} \quad \text{and} \quad \begin{pmatrix} \varrho_d \\ \gamma_d \\ \beta_d \end{pmatrix} = M_{Brad} \begin{pmatrix} X_d \\ Y_d \\ Z_d \end{pmatrix}. \tag{8}$$

where $X_sY_sZ_s$ are calculated with equation 6 by setting $R(\lambda)$=1. A scaling is thus achieved with the diagonal matrix

$$M_{\text{scale}} = \begin{pmatrix} \varrho_s/\varrho_d & 0 & 0 \\ 0 & \gamma_s/\gamma_d & 0 \\ 0 & 0 & \beta_s/\beta_d \end{pmatrix}. \tag{9}$$

Chromatic adaptation of the source illuminant *XYZ* tristimulus to the destination illuminant *X'Y'Z'* tristimulus is then obtained by a transformation to the cone response domain ($M_{\text{Brad}}$), scaling with the white points ($M_{\text{scale}}$), and transformation back to CIE tristimulus ($M_{\text{Brad}}^{-1}$):

$$\begin{pmatrix} X' \\ Y' \\ Z' \end{pmatrix} = M_{\text{Brad}}^{-1} M_{\text{scale}} M_{\text{Brad}} \begin{pmatrix} X \\ Y \\ Z \end{pmatrix} = M_{\text{ca}} \begin{pmatrix} X \\ Y \\ Z \end{pmatrix}. \tag{10}$$

**(iii)** Linear transformation of CIE *X'Y'Z'* (D65 illuminant) tristimulus values to linear sRGB color space by the following matrix multiplication (IEC 61966-2-1:1999):

$$\begin{pmatrix} R_{\text{lin}} \\ G_{\text{lin}} \\ B_{\text{lin}} \end{pmatrix} = \begin{pmatrix} 3.2404542 & -1.5371385 & -0.4985314 \\ -0.9692660 & 1.8760108 & 0.0415560 \\ 0.0556434 & -0.2040259 & 1.0572252 \end{pmatrix} \begin{pmatrix} X' \\ Y' \\ Z' \end{pmatrix}. \tag{11}$$

Finally, linear sRGB values can be transformed to printable and displayable sRGB digital values (between 0 and 1) with

$$\begin{pmatrix} R \\ G \\ B \end{pmatrix} = 1.055 \begin{pmatrix} R_{\text{lin}}^{1/\gamma} \\ G_{\text{lin}}^{1/\gamma} \\ B_{\text{lin}}^{1/\gamma} \end{pmatrix} - 0.055 \qquad \text{and} \qquad \begin{pmatrix} R \\ G \\ B \end{pmatrix} = 12.92 \begin{pmatrix} R_{\text{lin}} \\ G_{\text{lin}} \\ B_{\text{lin}} \end{pmatrix} \tag{12}$$

$$\text{for } R_{\text{lin}}, G_{\text{lin}}, B_{\text{lin}} > 0.0031308 \qquad \text{for } R_{\text{lin}}, G_{\text{lin}}, B_{\text{lin}} \leq 0.0031308$$

where $\gamma$=2.4. For an 8-bit image, an often used format, each individual *RGB* value per pixel has to be multiplied by $2^8$-1=255 and round to the nearest integer. Note that we recorded the optical images, calculated the colors, and display the images with $\gamma$=1 for better contrast and to avoid clipping of colors.

## 2.3 Comparison of the calculation and experimental data

Comparing colors in the *RGB* color space is quite difficult and is subjective according to human eye perception. The CIE *xyY* color space in turn allows an objective view of the *xy* chromaticities by avoiding the influence of luminance *Y*. Transformation to *xyY* color space is straightforward starting from the *XYZ* color space:

$$x = \frac{X'}{X' + Y' + Z'} \qquad \text{and} \qquad y = \frac{Y'}{X' + Y' + Z'}. \tag{13}$$

Figure S8 shows the *xy*-chromaticity diagram with the sRGB color space (black triangle), the experimental data (red crosses), and the simulation (blue lines) for thicknesses up to 160 nm. The values run clockwise, with increasing 2DP thickness, along an ellipse around the D65 white point. The path of the calculated chromaticities from the reflectance simulation through the *xyY* color space is very similar but shifted to the

lower left (blue, dotted curve). This is most likely caused by unknown conversions inside the camera or in the optical train of the microscope. The spectrum of the light source might also be slightly different as given from the manufacturer. Another source of error is the uncertainty of the $SiO_2$ thickness and the dispersion of the refractive index of the 2DP. The last two, however, would cause a deformation of the ellipse rather than a shift in color space. We therefore adjusted the source white point for chromatic adaptation via the Bradford matrix manually. The calculated source white point from equation 6 with $R(\lambda)$=1 is $X_sY_sZ_s$=(0.842, 1.000, 0.707), whereas the adjusted source white point matching the experimental data is found to be (0.838, 1.000, 0.865). The destination white point of D65 illuminant is $X_dY_dZ_d$=(0.950, 1.000, 1.089). The blue dashed curve in Fig. S8 shows the simulation using the adjusted white point. This curve is used in the following for linear *RGB*, contrast calculation, and the colorbars. Figure S9 shows the experimental and simulated linear *RGB*-values depending on thickness in a *xy*-graphical representation. With the model parameters used, $d_2(SiO_2)$=300 nm, *NA*=0.9, $n_1$(2DP)=1.68, and the adjusted source white point, a good agreement with the experimental values is achieved.

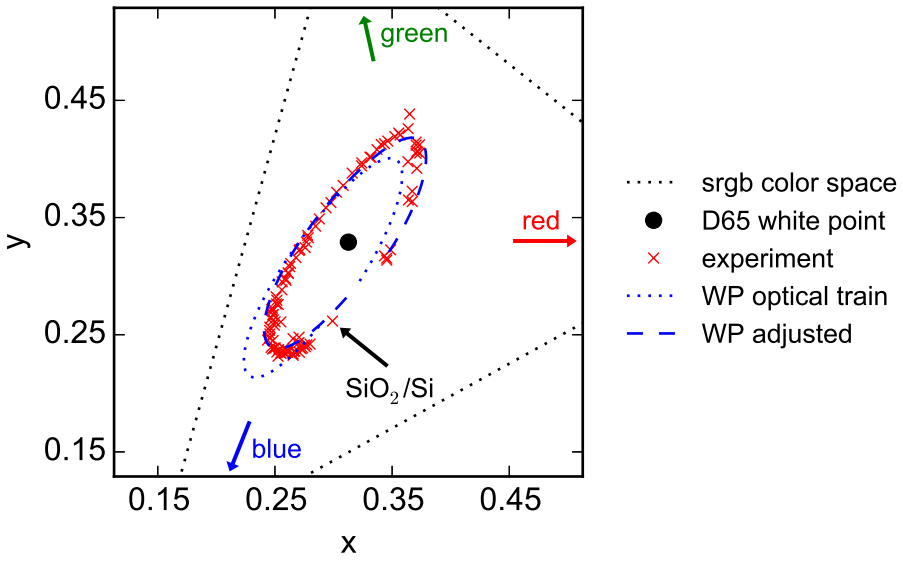


Figure S8: *xy*-chromaticity diagram illustrating the color difference of experimental and simulated reflectance colors of 2D polymers with thickness up to 160 nm on a $SiO_2$(300 nm)/Si substrate. The black triangle represents the sRGB color space with the D65 white point (black dot). The black arrow points to the color of the $SiO_2$(300 nm)/Si substrate. Thickness of the 2D polymer increases clockwise. Two simulations are shown, one using the white point (WP) from the optical train (blue dotted line) and one with a manually adjusted WP (blue dashed line).

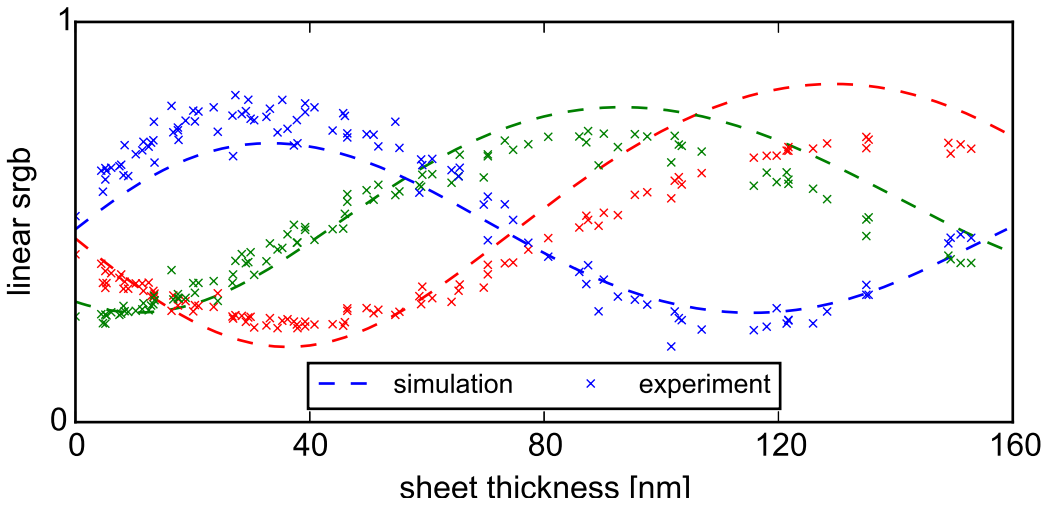


Figure S9: Experimental (crosses) and simulated (dashed lines) individual linear $R$, $G$, $B$ values drawn in their corresponding colors.

## 3 Determination of the lattice orientation

Lattice directions shown in Fig. 7 of the main text were extracted from 2D Fast Fourier Transforms (2DFFTs) of AFM-phase images. An example is shown in Fig. S10 where the phase image (flattened) is shown in a), and the Gaussian filtered 2DFFT of the raw phase image is shown in b). An algorithm locates intensity peaks and extracts corresponding angles $\varphi_{\mathrm{2DFFT}}$ with respect to the horizontal axis. The center of the 2DFFT represents the coarsest periodic distances of the real space image. Thus, real space distances between the grey dotted lines in Fig. S10c) appear as intensity peaks with distance $d_{\mathrm{2DFFT}}$ to the middle of the 2DFFT image. The real space lattice vectors have an angle $\varphi_{\mathrm{real}}=\varphi_{\mathrm{2DFFT}}+90°$ to the fast scan direction and a length $a_{\mathrm{real}}={d^{-1}}_{\mathrm{2DFFT}}/\cos 30°=2{d^{-1}}_{\mathrm{2DFFT}}/\sqrt{3}$. Note that the angles shown in Fig. 7 of the main text differ from the angles determined here by 21° due to rotational difference of the optical image and the fast scan direction of the AFM. The mean distance between neighbouring lattice positions $a_{\mathrm{real}}$ calculated by averaging over all images amounts to (1.99 ± 0.07) nm.

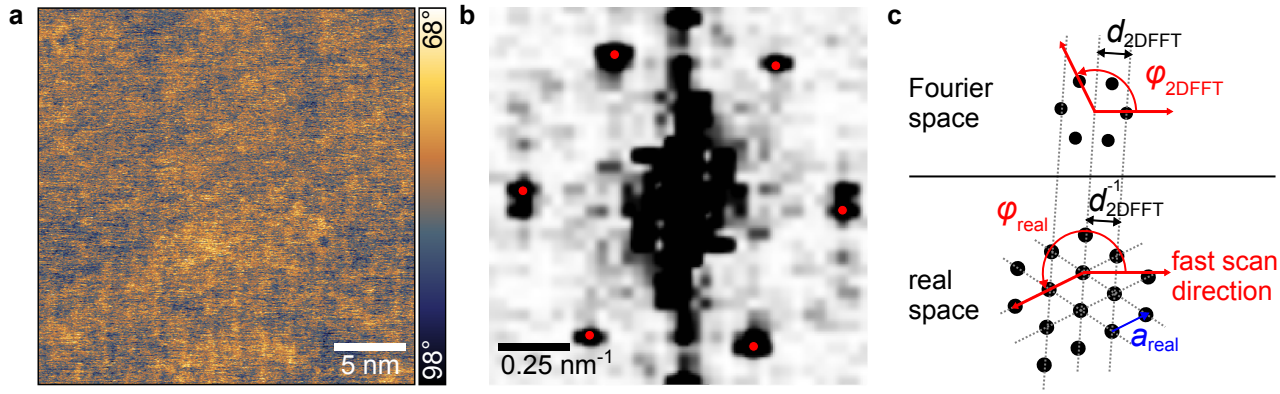


Figure S10: Determining lattice vectors from AFM-phase images. (a) Flattened AFM-phase image taken at one position of Fig. 7 of the main text. (b) Gaussian filtered 2DFFT (zoom) of the raw image with marked reciprocal lattice positions (red dots). (c) Illustration of the angle and distance conversion from Fourier space to real space. The Fourier space orientation is taken from the 2DFFT image shown in b). The distance between the grey dotted lines in real space is identical to the inverse distance between the center of the 2DFFT and the first order spots. Range of scanning parameters: AM-AFM (net-repulsive) $A_0$=4.5 nm to 6.0 nm, $A_{SP}$=0.6 nm to 0.9 nm.

## 4 Missing template molecule and tip change

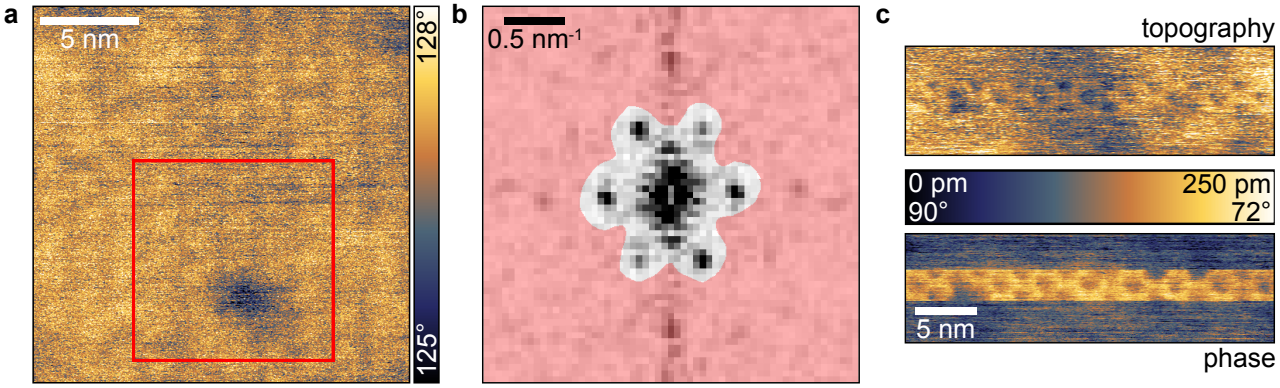


Figure S11: (a) Raw phase image of the 2DFFT filtered image shown in Fig. 8a) of the main text. The red box marks the area of the cropped image shown in the main text. (b) 2DFFT image of a). Higher frequencies and those close to the spots (red-shaded area) were filtered out for the image shown in Fig. 8a). (c) AM-AFM in the net-repulsive regime showing a sudden enhancement of the resolution caused by a change of the tip. Scanning parameters for c): AM-AFM (net-repulsive) $A_0$=7.0 nm, $A_{SP}$=4.7 nm.

## References


1 P. Blake, E. Hill, A. C. Neto, K. Novoselov, D. Jiang, R. Yang, T. Booth and A. Geim, *Appl. Phys. Lett.*, 2007, **91**, 063124.

2 M. Born and E. Wolf, *Principles of Optics*, Pergamon, 6th edn, 1980, pp. 1 – 70.

3 G. Ghosh, in *Handbook of Optical Constants of Solids*, ed. E. D. Palik and G. Ghosh, Academic Press, Burlington, 1997, vol. 5, ch. 2, pp. 5 – 114.

4 Refractive Index Database, http://www.filmetrics.com/refractive-index-database/, (accessed March 2016).

5 M. Bruna and S. Borini, *J. Phys. D: Appl. Phys.*, 2009, **42**, 175307.

6 Colour and Vision Research Laboratory: New CIE XYZ functions transformed from the CIE (2006) LMS functions, http://www.cvrl.org/ciexyzpr.htm, (accessed April 2016).

7 M. R. Luo and R. W. G. Hunt, *Color Res. Appl.*, 1998, **23**, 154–158.

8 Bruce Lindbloom: Chromatic Adaptation, http://www.brucelindbloom.com, (accessed June 2016).